Vertically coupled plasmonic slot waveguide cavity for localized biosensing applications

Ga¨el D. Osowiecki,* Elsie Barakat, Ali Naqavi and Hans Peter Herzig

Optics & Photonics Technology Laboratory, Institute of Microengineering (IMT), École Polytechnique Fédérale de Lausanne (EPFL), Rue de la Maladière 71b, CH-2002 Neuchâtel, Switzerland

**gael.osowiecki@epfl.ch*

Abstract: We propose and study an integrated refractive index sensor which is based on a plasmonic slot waveguide cavity. In this device, a guided mode supported by a silicon photonic wire waveguide is vertically coupled to a metal-dielectric-metal cavity separated by a silicon oxide spacer. We perform an in-depth study that links the geometrical parameters of the sensor to the coupling mechanism and sensitivity of the plasmonic slot waveguide cavity. Simulation results promise that local changes of refractive index can be measured with a high sensitivity of around 600 nm/RIU in a femto-liter volume. These results are obtained with three-dimensional time and frequency domain simulations. Thanks to the high field enhancement in the slot of the plasmonic cavity, a high local sensitivity to changes of refractive index is obtained. Moreover, the high level of achieved decoupling between the bulk and the local sensitivity complies well with the requirements of biomolecular sensing.

OCIS codes: (250.5403) Plasmonics; (230.7370) Waveguides; (130.6010) Sensors; (280.4788) Optical sensing and sensors; (280.1415) Biological sensing and sensors; (350.4238) Nanophotonics and photonic crystals.

References and links

1. J. A. Schuller, E. S. Barnard, W. Cai, Y. C. Jun, J. S. White, and M. L. Brongersma, "Plasmonics for extreme light concentration and manipulation," Nat. Mater. **9**, 193–204 (2010).
2. J. Homola, S. S. Yee, and G. Gauglitz, "Surface plasmon resonance sensors: review," Sensor. Actuat. B-Chem. **54**, 3–15 (1999).
3. J. Homola and J. Dostalek, *Surface plasmon resonance based sensors* (Springer, 2006), vol. 4.
4. A. Cosentino, Q. Tan, M. Roussey, and H. P. Herzig, "Refractive index sensor based on slot waveguide cavity," J. Europ. Opt. Soc. Rap. Public. **7**, 12039 (2012).
5. Q. Tan, A. Cosentino, M. Roussey, and H. P. Herzig, "Theoretical and experimental study of a 30nm metallic slot array," J. Opt. Soc. Am. B **28**, 1711–1715 (2011).
6. Y. Chen and H. Ming, "Review of surface plasmon resonance and localized surface plasmon resonance sensor," Photon. Sens. **2**, 37–49 (2012).
7. K. A. Willets and R. P. Van Duyne, "Localized surface plasmon resonance spectroscopy and sensing," Annu. Rev. Phys. Chem. **58**, 267–297 (2007).
8. K. M. Mayer and J. H. Hafner, "Localized surface plasmon resonance sensors," Chem. Rev. **111**, 3828–3857 (2011).
9. A. J. Haes and R. P. V. Duyne, "A unified view of propagating and localized surface plasmon resonance biosensors," Anal. Bioanal. Chem. **379**, 920–930 (2004).
10. Z. Han, A. Y. Elezzabi, and V. Van, "Experimental realization of subwavelength plasmonic slot waveguides on a silicon platform," Opt. Lett. **35**, 502–504 (2010).

#212006 - $15.00 USD Received 16 May 2014; revised 8 Aug 2014; accepted 9 Aug 2014; published 21 Aug 2014

11. J. Yang, C. Sauvan, A. Jouanin, S. Collin, J.-L. Pelouard, and P. Lalanne, "Ultrasmall metal-insulator-metal nanoresonators: impact of slow-wave effects on the quality factor," Opt. Express **20**, 16880–16891 (2012).
12. H. Choo, M.-K. Kim, M. Staffaroni, T. J. Seok, J. Bokor, S. Cabrini, P. J. Schuck, M. C. Wu, and E. Yablonovitch, "Nanofocusing in a metal-insulator-metal gap plasmon waveguide with a three-dimensional linear taper," Nat. Photonics **6**, 838–844 (2012).
13. E. N. Economou, "Surface plasmons in thin films," Phys. Rev. **182**, 539–554 (1969).
14. J. A. Dionne, L. A. Sweatlock, H. A. Atwater, and A. Polman, "Plasmon slot waveguides: Towards chip-scale propagation with subwavelength-scale localization," Phys. Rev. B **73**, 035407 (2006).
15. R. Yang and Z. Lu, "Subwavelength plasmonic waveguides and plasmonic materials," Int. J. Opt. **2012**, 1–12 (2012).
16. G. Veronis and S. Fan, "Modes of subwavelength plasmonic slot waveguides," J. Lightwave Technol. **25**, 2511 –2521 (2007).
17. G. Veronis and S. Fan, "Guided subwavelength plasmonic mode supported by a slot in a thin metal film," Opt. Lett. **30**, 3359–3361 (2005).
18. C. Delacour, S. Blaize, P. Grosse, J. M. Fedeli, A. Bruyant, R. Salas-Montiel, G. Lerondel, and A. Chelnokov, "Efficient directional coupling between silicon and copper plasmonic nanoslot waveguides: toward metal-oxide-silicon nanophotonics," Nano Lett. **10**, 2922–2926 (2010).
19. Y. Luo, M. Chamanzar, and A. Adibi, "Compact on-chip plasmonic light concentration based on a hybrid photonic-plasmonic structure," Opt. Express **21**, 1898–1910 (2013).
20. L. Feng, D. Van Orden, M. Abashin, Q.-J. Wang, Y.-F. Chen, V. Lomakin, and Y. Fainman, "Nanoscale optical field localization by resonantly focused plasmons," Opt. Express **17**, 4824–4832 (2009).
21. Y. Lu, G. L. Liu, J. Kim, Y. X. Mejia, and L. P. Lee, "Nanophotonic crescent moon structures with sharp edge for ultrasensitive biomolecular detection by local electromagnetic field enhancement effect," Nano Lett. **5**, 119–124 (2005).
22. G. Veronis and S. Fan, "Compact couplers between dielectric and plasmonic slot waveguides," Proc. SPIE **6475**, 64750S (2007).
23. P. Holzmeister, G. P. Acuna, D. Grohmann, and P. Tinnefeld, "Breaking the concentration limit of optical single-molecule detection," Chem. Soc. Rev. **43**, 1014–1028 (2013).
24. P. Tinnefeld, "Single-molecule detection: Breaking the concentration barrier," Nat. Nano. **8**, 480–482 (2013).
25. P. B. Johnson and R.-W. Christy, "Optical constants of the noble metals," Phys. Rev. B **6**, 4370 (1972).
26. P. Berini, "Plasmon-polariton waves guided by thin lossy metal films of finite width: Bound modes of symmetric structures," Phys. Rev. B **61**, 10484–10503 (2000).
27. W.-P. Huang, "Coupled-mode theory for optical waveguides: an overview," J. Opt. Soc. Am. A **11**, 963–983 (1994).
28. G. W. Cong, K. Suzuki, S. H. Kim, K. Tanizawa, S. Namiki, and H. Kawashima, "Demonstration of a 3-dB directional coupler with enhanced robustness to gap variations for silicon wire waveguides," Opt. Express **22**, 2051–2059 (2014).
29. L. J. Sherry, R. Jin, C. A. Mirkin, G. C. Schatz, and R. P. Van Duyne, "Localized surface plasmon resonance spectroscopy of single silver triangular nanoprisms," Nano Lett. **6**, 2060–2065 (2006).

1. Introduction

The ability of metal-dielectric interfaces to sustain localized electromagnetic modes known as surface plasmon polaritons (SPP) allows confinement and guiding light in volumes smaller than the diffraction limit over a couple of micrometers in the visible spectrum. Thanks to these properties, recent scientific and practical interest in SPP optoelectronics has emerged [1]. Surface plasmon resonance (SPR) sensors [2] have been significantly successful in sensing refractive index changes over large surfaces. These SPR sensors can be used in different applications, for example to monitor the evolution of the binding reactions of specific molecules such as proteins over time. The operation of the mentioned sensors is based on the change of either wavelength or angle of the SPP resonance. Remarkable effort has been put into providing a higher throughput and multiplexing the detection process, mainly by using microfluidic systems [3].

In this paper we propose a geometry, based on a plasmonic slot waveguide cavity, that enables a significant improvement of highly multiplexed detection on an integrated silicon platform [4, 5]. Due to the large enhancement of the electromagnetic field by the SPP, the sensing volume is highly reduced, which allows localized detection of molecules in

#212006 - $15.00 USD Received 16 May 2014; revised 8 Aug 2014; accepted 9 Aug 2014; published 21 Aug 2014

sub-attoliter volumes. We expect our proposed device to be able to detect fluctuations of refractive index induced by a couple of molecules only. Similar results were obtained by localized surface plasmon resonance (LSPR) supported by metallic nanoparticles [6, 7] which reveals that for small molecule detection, LSPR can excel SPR because it is more sensitive to changes in refractive index close to its surface [8]. LSPR generally provides smaller bulk sensitivity values compared to SPR but the small detection volume of the LSPR enables an easier differentiation between bulk and surface refractive index changes and thus promotes a better detection of small molecules with a reduced noise from the bulk [9].

We consider the application of a plasmonic slot waveguide (PSW) in our proposed device. A PSW allows an easy integration in wafer-level micro-fabrication thanks to its planar geometry [10]. Metal-dielectric-metal structures like PSWs show deep sub-wavelength localization and enhancement of EM fields [11, 12]. The modal characteristics of PSWs have been extensively studied for semi-infinite metal-insulator-metal (MIM) films [13–15] as well as for truncated MIM films [16] from infrared to optical frequencies. The PSWs support a fundamental quasi-TEM mode at a large frequency range if the slot width is small enough compared to the wavelength [17]. It has been shown that such waveguides are major candidates for future on-chip interconnects as they allow dense integration and short coupling length to dielectric waveguides [18].

Our proposed hybrid plasmonic-dielectric sensor provides the possibility to bring and focus the light at the desired location on a planar surface to detect and analyze the bindings of small molecules. Similar works have been done recently to concentrate light at a desired position [19–21]. The core of our sensor is a plasmonic slot waveguide cavity (PSWC) which behaves similarly to a Fabry-Pérot resonator and has a resonant wavelength sensitive to the surrounding refractive index [22]. The small volume of the resonating cavity enables a refractive index sensing in sub attoliter volumes, which is of great interest for bio-molecular sensing especially when it comes to breaking the concentration limit of optical single molecule detection [23, 24]. The refractive index change can be obtained by measuring the shift of the resonant wavelength in the transmitted spectrum or at a single wavelength by measuring the transmitted intensity change.

This paper is divided into three parts. The first part gives a description of the structure of the proposed sensor with its geometrical parameters and their effect on the transmission spectrum. The second part is devoted to the investigation of the different guided modes that are present in the structure and their coupling to each other, which is linked to the resonance condition. The third part discusses the strong field enhancement by the PSWC and its excellent ability to sense refractive index changes either in the bulk or at its surface.

2. Plasmonic slot waveguide cavity (PSWC) on a single mode waveguide

The integrated plasmonic cavity is depicted in Fig. 1. It lays on top of a silicon oxide spacer layer and a silicon waveguide. The silicon waveguide is designed in order to support only two modes in the near infrared wavelength range between 1200 nm and 1700 nm. Based on the field profiles, the fundamental quasi-TE mode of the silicon waveguide is the only mode being able to excite the PSWC modes contrarily to the fundamental quasi-TM mode. The silicon waveguide has a thickness of 220 nm and a width of 450 nm, and is used to guide light from the source to the cavity and from the cavity back into the waveguide to the detector.

The transmission spectrum is measured at the output of the silicon waveguide and depends on its geometrical parameters: the cavity length (L), the metal thickness (t_m), the spacer thickness (t_s) and the slot width (w_s), shown in Fig. 1. In order to have an idea of the influence of these parameters on the resonant optical properties of the device, we primarily calculate the transmission spectrum for different lengths of the PSWC. Then we investigate the impact of

#212006 - $15.00 USD Received 16 May 2014; revised 8 Aug 2014; accepted 9 Aug 2014; published 21 Aug 2014

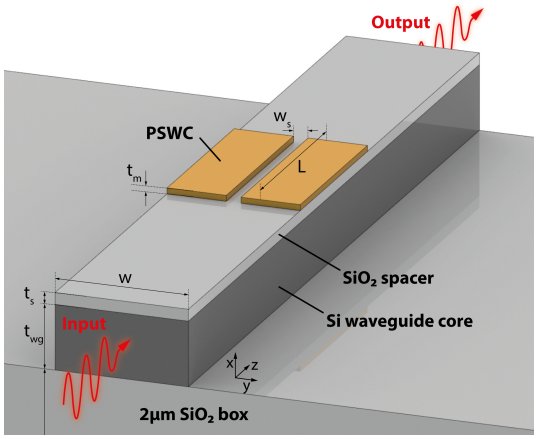

Fig. 1. Drawing of the hybrid photonic-plasmonic cavity. On top of a single crystal silicon waveguide there is a plasmonic slot waveguide cavity which is separated from it by a silicon oxide film. Invariant spatial parameters of this structure are $t_{wg} = 220nm$, $w = 450nm$ and $w_s = 50nm$. Variable spatial parameters of the PSWC are $L = 600nm$, $t_s = 40nm$ and $t_m = 20nm$

the coupling changes on the resonance properties by changing the oxide spacer thickness (t_s). We perform our numerical study with the commercial software CST Microwave using frequency and time domain calculations. A non-uniform three dimensional hexahedral meshing is applied in x, y, and z directions in order to define the structure. The grid size varies continuously between 2 nm for the plasmonic cavity and 26 nm for the silicon waveguide over a bounding box of $2.3\,\mu m(\mathrm{X}) \times 2\,\mu m(\mathrm{Y}) \times 2.7\,\mu m(\mathrm{Z})$ containing 6 billion of mesh cells. The temporal step for FDTD is set to $4.5 \times 10^{-18} s$. We use a perfectly matched layer (PML) of 8 layers as an artificial absorbing boundary. Metal dispersion is an 4^{th}-order polynomial fit of Johnson and Christy data [25]. To reduce computation time, we use a distributed computing feature of the software package.

Figure 2(a) demonstrates transmission versus the cavity length (L). It shows multiple transmission peaks that appear at wavelengths corresponding to the longitudinal resonances of the cavity. As expected, the resonance positions strongly depend on the cavity length. The resonance peaks shift to a larger wavelength (red shift) as the cavity length increases. In the bandwidth from λ = 1200nm to 1700nm, the fundamental resonance disappears for cavity lengths smaller than 250 nm. This is due to phase-matching which cannot be obtained for cavity lengths smaller than $\lambda_{eff}/2$, where λ_{eff} is the effective wavelength of the fundamental guided mode inside the PSW. Moreover, below 1200nm the silicon waveguide becomes multimode and the resonance starts to be affected by other modes. Figure 2(a) shows that higher order resonances appear for longer cavities. The dashed black line corresponds to the cavity length where the first harmonic of the resonance is located at around $\lambda = 1.5\,\mu m$.

Figure 2(b) represent the transmission as function of the silicon oxide spacer thickness. The resonant wavelength position of the first harmonic occurs at around λ = 1550 nm and remains almost independent of the spacer thickness changes. The spacer thickness, which separates the PSWC and the waveguide, affects the coupling efficiency between the mode of the waveguide and the cavity mode. Due to the presence of the spacer all along the silicon waveguide, changing the spacer thickness affects slightly the effective index of the guided mode present in the silicon waveguide. Due to fabrication restrictions, a slot width of $t_s = 50\,nm$ is chosen for our design. From these calculations, we opted for the following parameters: $t_m = 20\ nm$, $w_s = 50\ nm$,

#212006 - $15.00 USD Received 16 May 2014; revised 8 Aug 2014; accepted 9 Aug 2014; published 21 Aug 2014

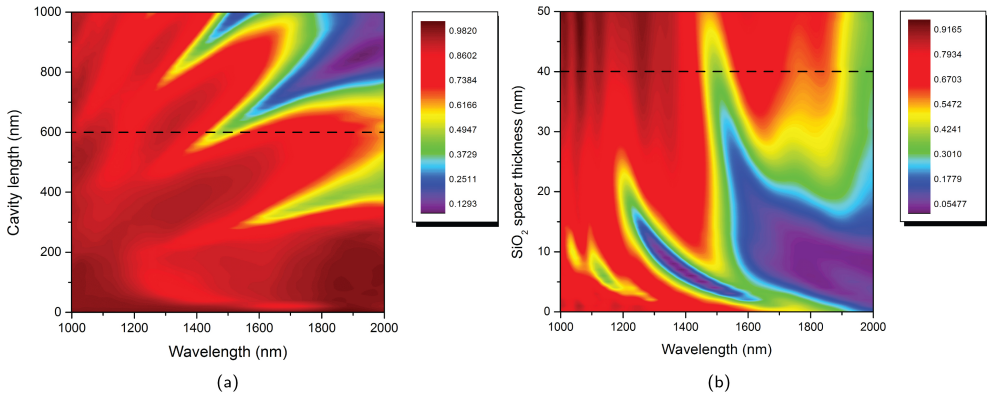

Fig. 2. (a): Dependence of the transmission spectra as function of the cavity length. (b): Dependence of the transmission spectra as function of the spacer thickness. Both figures exhibit typical Fabry-Pérot resonance peaks.

$L = 600\ nm$, and $t_s = 40\ nm$. Using the latter geometrical parameters the first harmonic resonance is excited at the wavelength of around $\lambda = 1.5\,\mu m$ and has a high extinction ratio of about 3 which makes the resonance position easily measurable.

3. Light management in the PSWC

3.1. Modal analysis

It is desired to strongly confine and enhance the E-field in the slot that is created by the two metallic pads. As the PSWC is excited by a dielectric waveguide, we need to perform a modal analysis of the dielectric waveguide itself and of the coupled system i.e. the dielectric waveguide coupled to the plasmonic slot waveguide to optimize it. We assume that the plasmonic cavity is excited by a single quasi-transverse-electric (qTE) mode travelling in a silicon wire waveguide at wavelengths from 1200 nm to 1700 nm. Transverse electric is the case where the polarization of the electric field vector is perpendicular to the x,z-plane like in Fig. 3(a). We perform a systematic analysis of the coupling in the weak coupling regime. From coupled-mode theory, a mode analysis of the uncoupled waveguide is made to describe the coupled waveguide, as suggested by Ref. [26]. We calculated the uncoupled and coupled modes with the 2D CST mode solver. Figure 3(a) shows the E_y-field amplitude of the qTE mode of the silicon wire waveguide used to excite the PSWC. In Fig. 3(b) we show the E_y-field amplitude of the uncoupled fundamental plasmonic slot waveguide mode in which the silicon core has been replaced by silicon oxide. As a result of a good mode matching between qTE and A_0 modes, two hybrid modes which are the superposition of the qTE and A_0 modes are excited. In Figs. 3(c) and 3(d) the two calculated hybrid modes are depicted, which are the result of the coupling between the PSW and the silicon waveguide (H_{TE_0} and H_{TE_1}). The two hybrid modes keep the high field localisation which is characteristic to the A_0 slot mode.

3.2. PSWC coupling

Light coupling from the dielectric waveguide to the PSW plays an important role in the performance of our sensor. The proposed cavity is in fact a PSW with a length of only 600 nm, which is shorter than the coupling length between the silicon waveguide and the PSW. Similar to two coupled dielectric waveguides, the two hybrid modes H_{TE_0} and H_{TE_1} of the described structures have two different propagation constants $\beta_{H_{TE_0}}$ and $\beta_{H_{TE_0}}$, which lead to

#212006 - $15.00 USD Received 16 May 2014; revised 8 Aug 2014; accepted 9 Aug 2014; published 21 Aug 2014

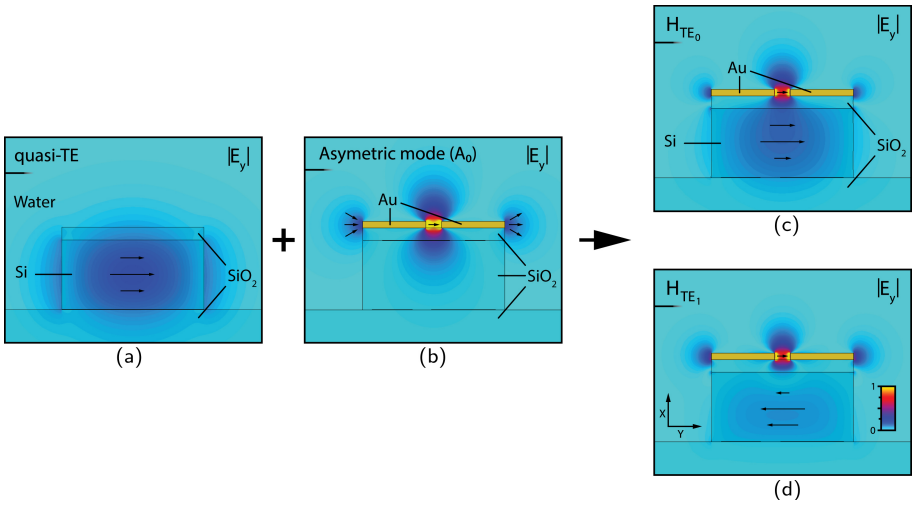

Fig. 3. 2D E_y-field amplitude component at $\lambda = 1500nm$. (a): Quasi-TE mode of the silicon waveguide with its SiO_2 spacer ($t_s = 40nm$, $w = 450nm$). (b): Uncoupled asymmetric PSW fundamental mode (A_0) with the waveguide core material replaced by silicon oxide ($t_m = 20nm$). (c) and (d): H_{TE_0} and H_{TE_1} hybrid modes of the PSW coupled to the silicon waveguide.

interferences during their propagation. Consequently for an infinitely long PSW, an alternating energy transfer from the dielectric waveguide to the PSW and vice versa is observed. The coupling length is equal to [27]:

$$L_c = \frac{\pi}{\beta_{H_{TE_0}} - \beta_{H_{TE_1}}} \tag{1}$$

where L_c corresponds to the length where a total transfer of the energy from one waveguide to the other one occurs. For the given structure, at $\lambda = 1.6\,\mu m$ the effective index is 2.54 and 2.09 for the H_{TE_0} and H_{TE_1} modes respectively; these values result in a coupling length of approximately $1.78\,\mu m$ [Fig. 3]. The coupling length of the proposed structure is more than an order of magnitude smaller than that of a conventional silicon wire waveguide directional coupler [28]. To reduce the coupling length, the difference between the propagation constants of both hybrid modes need to be increased. In addition to bio-sensing, this extremely short coupling length is of great interest to save as much space as possible on future photonics integrated interconnects and circuits. The propagation constants and the field distributions of the shown modes are calculated using the CST Microwave 2D mode solver and the coupling length is calculated with the use of the Eq. (1). The coupling length depends strongly on the geometrical parameters of the structure. When increasing the spacer thickness, the interaction of the evanescent tails of both modes is reduced and thus the coupling length is increased. On the other side, shrinking the size of the silicon wire waveguide will shorten the coupling length because the evanescent tail of the silicon wire waveguide mode will interact more with the PSW mode.

In order to confirm the coupling length calculations according to Eq. (1), a rigorous calculation based on the 3D frequency-domain solver of CST Microwave is done. Figure 4(a) shows the distribution of the E_x component of the electric field for a structure excited from the left side by the qTE mode of the silicon waveguide at $1.6\,\mu m$ wavelength. After one micrometer the mode starts to couple into an infinitely long PSW. The mode of the silicon

#212006 - $15.00 USD Received 16 May 2014; revised 8 Aug 2014; accepted 9 Aug 2014; published 21 Aug 2014

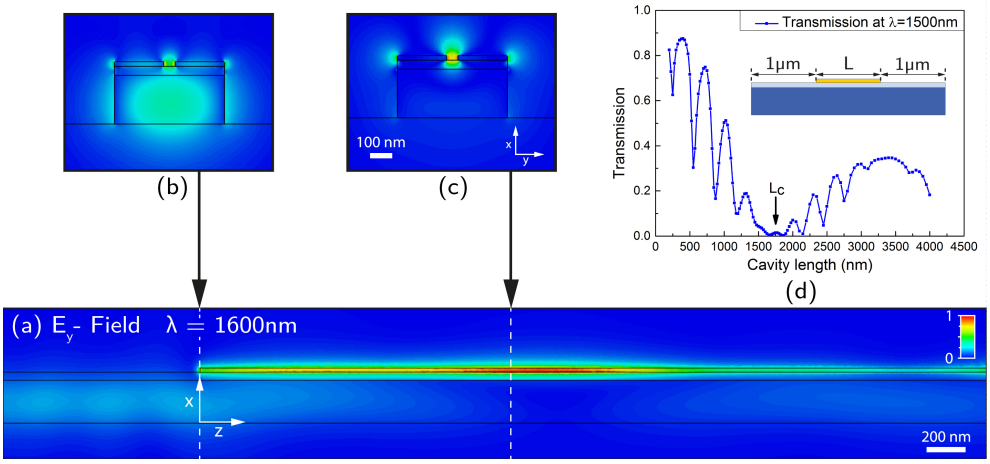

Fig. 4. (a): E_y-field amplitude showing the coupling between the dielectric waveguide and the metallic slot calculated with 3D frequency-domain solver of CST Microwave. (b) and (c): E_y-field amplitude of the 2D mode profile at $z = 0$ and $z = 1.78\mu m$. (d): Transmission of the excited cavity as function of the cavity length at $\lambda = 1500nm$.

waveguide is coupled into the metallic slot after a coupling length of about $1.78\,\mu m$. At L_c, the total energy density is transferred to the slot where the electric field is confined and the energy is coupled back to the silicon waveguide at $2 \times L_c$. The obtained L_c value shows good agreement with the mode coupling analysis described previously. This confirms that the device works in the weak coupling regime. The inset of Figs. 4(b) and (c) shows the mode field distribution at $z = 0$ and $z = L_c$ respectively. at $z = 0$ light is essentially confined in the silicon core while at L_c light is confined in the sub-wavelength-sized slot. Figure 4(d) shows the transmission as a function of the cavity length at the wavelength of 1.5 μm. The inset of Fig. 4(d) shows a sketch of the structure which is composed by an input and an output silicon waveguide of $1\,\mu m$ length and the PSWC of length L in the middle. In contrast to the structure which was infinitely long, this one is a PSW cavity, thus the metallic slot has a finite length which is varied to observe its impact on transmission. Two types of oscillations appear in the transmission. The one with shorter period corresponds to the cavity resonance due to the reflection of the light at both ends of the slot. The one with a longer period originates from the interference between the two propagating modes which have different propagation constants (β_{HTE_0} and β_{HTE_1}). The coupling length of the structure can thus be retrieved from the transmission spectrum. At the coupling length, minimum of transmission occurs. In our case, $L_c = 1.75\,\mu m$ which agrees with the result of Eq. (1) and the rigorous simulation. Another mechanism which is affecting the coupling is the change of the refractive index of the outer medium. The silicon waveguide mode effective index is dependent on the outer medium's refractive index, thus the coupling condition to the PSWC are changing. Because this coupling perturbation is relatively small it will be neglected in the next section when calculating the bulk sensitivity of the PSWC.

4. Field enhancement and sensitivity

In this section we discuss the near field enhancement around the PSWC and its dependance on bulk and localized sensitivity to refractive index changes. The bulk refractive index sensitivity is achieved by simulating the resonance peak shift ($\Delta\lambda$) obtained by the change of refractive index (Δn) of the whole medium around the PSWC. The sensitivity is defined as $S = \Delta\lambda/\Delta n$.

#212006 - $15.00 USD Received 16 May 2014; revised 8 Aug 2014; accepted 9 Aug 2014; published 21 Aug 2014

Likewise, the local sensitivity is obtained by simulating a change of the refractive index of only a thin layer of a couple of nanometer wrapped around the PSWC.

4.1. *Field enhancement*

The ability to detect small molecules in the vicinity of the PSWC is proportional to it's field enhancement. Equation (2) expresses the average normalized E-field intensity enhancement due to the presence of the PSWC. It is obtained by the ratio of - the integration of $|\mathbf{E}|^2$ over a volume V including the PSWC - over the same integration calculated in the same volume but without the effect of the metallic cavity. The integration volume V is a box centered on the PSWC with dimensions: $[t_m + 40nm]$ (X) $\times$ $[w + 40nm]$ (Y) $\times$ $[L + 40nm]$ (Z).

$$FE = \frac{\iiint\limits_V |\mathbf{E}_{cav}|^2 \, \mathrm{d}x \, \mathrm{d}y \, \mathrm{d}z}{\iiint\limits_V |\mathbf{E}_{wg}|^2 \, \mathrm{d}x \, \mathrm{d}y \, \mathrm{d}z} \tag{2}$$

In Fig. 5(a), we display the field enhancement of a gold PSWC of 600 nm length (in red) as a function of the wavelength compared to its transmission spectrum (in blue). The maximum field intensity enhancement occurs at the longitudinal resonance of the H_{TE_0} guided mode. In addition, we observe that at higher harmonics (i.e. for longer cavities at the same wavelength), the field enhancement increases. This is due to the length of the cavity, which is increasing and approaching the coupling length L_c, thus more light is coupled to the cavity. In Fig. 5(b) the same electric field intensity enhancement is shown on a plane cutting the PSWC at half of its thickness. It is observed that light is essentially confined between the two metallic interfaces. This is due to the excitation of a guided plasmonic mode inside the cavity which propagates from the bottom to the top on Fig. 5(b). Nevertheless, one can see some higher field intensities at the outer side of the cavity, which are mainly due to the presence of the H_{TE_1} mode.

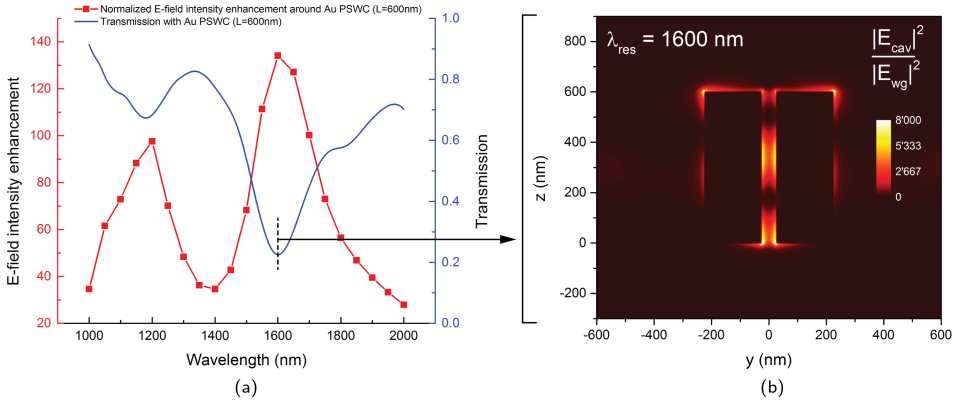

Fig. 5. (a): Transmission spectrum compared to the averaged E-field enhancement around a gold PSWC ($t_s = 40nm$, $w = 450nm$, $t_m = 20nm$, $w_s = 50nm$, $L = 600nm$). (b): 2D normalized $|E|^2$ field distribution at half the metal thickness of the plasmonic cavity at resonance frequency.

4.2. *Bulk and local sensitivity*

Likewise, we performed a sensitivity study of the structure with three different metals - gold, silver, and aluminum - to find the relation between near-field intensity enhancement and

#212006 - $15.00 USD Received 16 May 2014; revised 8 Aug 2014; accepted 9 Aug 2014; published 21 Aug 2014

detection of localized changes of refractive index. It was shown in section 2 that changing the spacer thickness does not vary the resonant wavelength but it significantly modifies the coupling between the waveguide and the plasmonic cavity. Because we want to keep the cavity as small as possible, we study the sensitivity of the PSWC as a function of the spacer thickness for the three different metals. The dispersion of the different metals is described using the data given by Johnson and Christy [25]. To calculate the bulk sensitivity as explained earlier in the beginning of section 4, two FDTD simulations were performed with refractive index of the outer medium changing from 1.32 (water at 1500 nm) to 1.35 (acetone at 1500 nm).

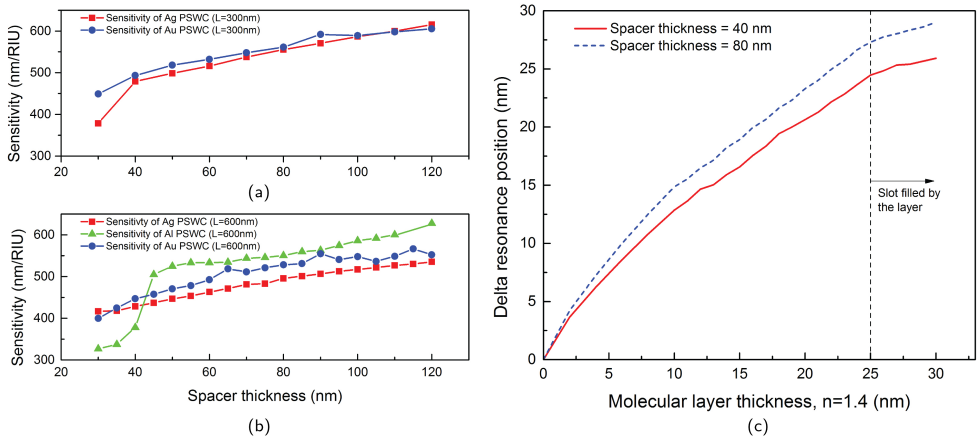

Fig. 6. (a): Bulk sensitivity for silver and gold PSWC of 300 nm length as function of the spacer thickness. (b): Bulk sensitivity for silver, gold and aluminium PSWC of 600 nm length as function of the spacer thickness. (c): Resonance wavelength shift of a 600 nm (L) long gold PSWC as a function of the thickness of a molecular layer of refractive index of 1.4 deposited on it.

Figure 6(a) shows the bulk sensitivity as function of the spacer thickness for a 300 nm long PSWC made out of silver or gold. Figure 6(b) shows a similar result for a 600 nm long PSWC made out of silver, gold or aluminium. The resonant wavelength of the PSWC on Figs. 6(a) and 6(b) are both around λ_{res} = 1500 nm; thus the fundamental resonance is excited for the 300 nm long PSWC, and the first harmonic is excited for the 600 nm long PSWC. Note that on Fig. 6(a) the aluminium PSWC sensitivity is missing because the extinction ratio of the resonance is too small. On Figs. 6(a) and 6(b) we observe a general increase of the bulk sensitivity for all the three metals for increasing spacer thicknesses. For the silver PSWC on Fig. 6(a), the bulk sensitivity reaches up to 615 nm/RIU for a spacer thickness of 120 nm and a cavity length of 300 nm. It shows that the fundamental resonance has a higher bulk sensitivity than the first-order resonance. Moreover, when using the fundamental resonance, the detection volume becomes smaller which is better for single molecule sensing at high concentration [24]. With increasing spacer thicknesses the fundamental resonance extinction ratio decreases, thus tracking the resonance becomes more difficult. The results of Figs. 6(a) and 6(b) show that the less coupled the system is, the stronger the resonance wavelength will be perturbed by a certain refractive index change of the bulk. However, for aluminum, even if the bulk sensitivity is higher, the quality factor and the extinction ratio are smaller because of the high amount of loss in the aluminum; this strongly affects the detection limit of the sensor. Using silver for the cavity provides the highest quality factors and thus the highest photon life time in the cavity and the highest local field enhancement.

The bulk sensitivity values obtained by our simulations are only 40% lower than the result

#212006 - $15.00 USD Received 16 May 2014; revised 8 Aug 2014; accepted 9 Aug 2014; published 21 Aug 2014

shown in [4] where a periodic array of PSWC is used on top of a slab waveguide which also has a 30 times larger interaction volume.

As the goal of this sensor is to detect the binding of small molecules to its surface, a high bulk sensitivity might create a lot of noise to the detection e.g. temperature fluctuations. Therefore it is important to study how surface sensitive this sensor is. In order to investigate surface or local sensitivity, we performed a resonance position tracking for different thicknesses of a molecular layer of refractive index equal to 1.4 around the gold PSWC. In Fig. 6(c), the shift of the resonant wavelength is shown for a molecular layer thickness growing from 0 to 30 nm for a gold PSWC with the same geometrical parameters as the one shown on Fig. 5. When changing the spacer thickness from 40 nm to 80 nm an increase in the local sensitivity is observed. For thin layers the sensitivity is extremely high, since it is related to the field intensity located in the slot of the cavity. Both field intensities and local sensitivities decreases the further we are from the metal surface. We believe that the high local sensitivity combined to the unique excitation of this plasmonic sensor can rival single particle LSPRs and be more easily multiplexed.

The performance of the sensor can be benchmarked by a figure of merit (FOM) expressed by the ratio of the sensitivity over the full width half maximum (FWHM) of the resonance. In the case of LSPR the best FOM is around 3 and the sensitivity ranges around 200 nm/RIU [29]. With a FOM of 4.1 for a spacer thickness of 40 nm, our sensor outperforms LSPR sensors.

Experimental realization of the mentioned plasmonic sensor is to be presented in a future publication.

5. Conclusion

We presented a theoretical study of a plasmonic slot waveguide cavity (PSWC) sensor which is a good candidate to detect changes in refractive index in sub-attoliter volumes with a high surface sensitivity. The sensor is excited by a silicon waveguide which gives flexibility in multiplexing the cavity on the chip surface for higher throughput. First we investigated the dependence of the spectral transmission, and specifically the resonance wavelength, on several sensor geometrical parameters such as the thickness of the spacer or the cavity length. Then we performed a modal analysis based on the coupled mode theory in order to describe the hybrid modes present in the cavity. Using this analysis we discussed the transmission modulation of the plasmonic slot waveguide cavity. This extra modulation is due to the presence of two propagating hybrid modes inside the cavity interfering with each other. Based on our simulations, a maximum field intensity enhancement of 8000 is obtained inside the slot at the resonance wavelength for a silver PSWC (λ = 1600 nm). This strong near field enhancement is the reason of the high sensitivity of our sensor and it could be beneficial to improve fluorescence detection or Raman scattering. We studied the sensor bulk and local sensitivity. Our simulations of the bulk sensitivity as function of the spacer thickness showed that for a weakly coupled PSWC, a higher quality factor and a higher bulk sensitivity are expected. A comparison study between different metals shows that silver and gold have a higher extinction ratio and a smaller detection limit due to their lower loss in the working wavelength range. And finally, by simulations, we showed that this sensor has a high local sensitivity. A resonance wavelength shift of 3nm is obtained for the deposition of a 1nm thick monolayer over the PSWC. This last result is of great importance for the detection of very small molecules and even single molecule sensing.

Acknowledgments

The authors acknowledge support from the Swiss National Science Foundation in the frame of OPICS project 200020-132461.